

# Aerial Manipulator Force Control Using Control Barrier Functions

Dimitris Chaikalis<sup>1</sup>, Vinicius Gonçalves<sup>2</sup>, Anthony Tzes<sup>2,3</sup> and Farshad Khorrami<sup>1,2</sup>

**Abstract**—This article studies the problem of applying normal forces on a surface, using an underactuated aerial vehicle equipped with a dexterous robotic arm. A force-motion high-level controller is designed based on a Lyapunov function encompassing alignment and exerted force errors. This controller is coupled with a Control Barrier Function constraint under an optimization scheme using Quadratic Programming. This aims to enforce a prescribed relationship between the approaching motion for the end-effector and its alignment with the surface, thus ensuring safe operation. An adaptive low-level controller is devised for the aerial vehicle, capable of tracking velocity commands generated by the high-level controller. Simulations are presented to demonstrate the force exertion stability and safety of the controller in cases of large disturbances.

## I. INTRODUCTION

Aerial platforms capable of autonomous task execution, safe operation and interaction with their environment, occasionally referred to as aerial workers [1], promise to increase efficiency and safety in tasks such as inspection [2], and transportation [3]. Typical multirotor vehicles equipped with planar motors are extensively used due to their availability in various sizes and development of high-fidelity sensors enabling operation in diverse indoor or outdoor settings and being robust to surrounding environments

Underactuation due to the planar placement of rotors leads to a coupling of the vehicle's altitude to its attitude. A common approach to re-instating the degrees of freedom lost due to underactuation, while also providing the vehicle with a method for interacting with its environment, is the attachment of robotic arms on the aerial vehicle. Such systems are sometimes referred to as aerial manipulators [4].

Aerial manipulators are capable of interacting with other entities via exchanging forces. Force control techniques can be used to solve a variety of problems, such as multi-robot cooperation by regulating either physical [4] or virtual forces [5] being exchanged. Likewise, the force control problem of regulating force exchanged with the environment can be used to solve problems such as automated push-pull and robotic grasping.

The problem of force exertion using fixed-base robotic manipulators has been thoroughly investigated [6], and can be extended to aerial manipulators using floating-base platforms [7].

Impedance control techniques control the interaction of aerial manipulators with the environment [8] in standalone

or coordinated cases [9], [10]. This area has been addressed in space robotics while interacting with floating objects [11].

Along these lines, this article studies the problem of exerting prescribed normal forces on planar surfaces, with a multirotor aerial vehicle coupled with a dexterous robotic arm. The problem of sustained force exertion has applicability in tasks such as contact inspection, autonomous pushing, or clearing an area of obstacles, and in space robotics [12], [13].

In [14], a system is presented for force exertion applicable only for horizontal forces. The system consists of an aerial vehicle and a single DoF tool, with an additional slider at the end-effector, aimed at allowing friction-less sliding along one unconstrained axis of the surface.

An application on the peg-in-hole problem [15] is handled with a dual-arm manipulator for increased manipulability and simple controllers. In [16] the authors use a similar platform, with an eye-in-hand camera for achieving contact on a surface enriched with fixed visual features, enabling the control to take place in the image space. In [17] a fully-actuated vehicle is used, allowing for increased mobility during interaction, while the distance between end-effector and environment is used to aid the controller in achieving compliance. The model predictive control architecture is employed in [18], [19] for achieving force exertion with the environment, demanding accurate knowledge of the underlying dynamics.

In this work, it is desired for the force exertion to be perpetrated on a selected location of a surface and exclusively along its normal axis. With the interest of ensuring safety during the interaction task, an optimization-based controller is developed, incorporating control barrier functions (CBF) in its design [20]. The driving controller utilises kinematics of the vehicle and the robotic arm and outputs system-level velocity commands, allowing the developed scheme to be applicable to any type of multirotor platform and robot manipulator. The CBF is coupled with the driving controller via an optimization problem (using Quadratic Programming (QP)), aiming to guarantee that a desired relation between distance to the surface and end-effector alignment is maintained at all times. This ensures that contact with the environment will occur only under strict performance requirements, albeit in a continuous control manner.

This paper is structured as follows. Section II presents the model of the aerial manipulator and the environment, while also describing the task definition. Section III outlines the overall proposed optimization-based control design with the low-level controller for the aerial vehicle's stability in Section IV. Simulation studies are presented in Section V

<sup>1</sup>New York University, Electrical & Computer Engineering, Brooklyn, NY 11201, USA.

<sup>2</sup>NYUAD Center for Artificial Intelligence and Robotics, UAE

<sup>3</sup>New York University Abu Dhabi (NYUAD), Electrical Engineering, Abu Dhabi 129188, UAE

Corresponding author's email dimitris.chaikalis@nyu.edu

validating the approach, while concluding remarks appear in Section VI.

## II. PROBLEM STATEMENT & SYSTEM MODEL

The studied Unmanned Aerial Manipulator (UAM) system consists of an underactuated multirotor aerial vehicle coupled with a robotic arm with revolute joints, shown in Figure 1.

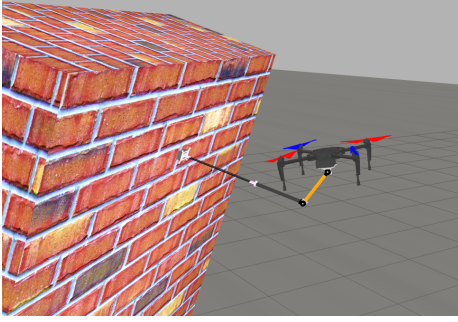


Fig. 1. Example Unmanned Aerial Manipulator (UAM) system. There exists a stationary planar surface, on which it is desired to exert normal forces. The relevant frames for the studied problem are:  $\mathcal{U}$  the frame fixed on the center of the aerial vehicle,  $\mathcal{E}$  the frame of the force sensor attached on the robotic arm end-effector,  $\mathcal{W}$  the world-fixed inertial frame and  $\mathcal{P}$  the inertial frame attached on the wall. It is assumed that the  $\tilde{z}$  vector of frame  $\mathcal{P}$  is normal to the wall, directed outside the wall with its center on the surface of the wall. Furthermore, it is assumed that the end-effector tool that will perform the force-exertion is aligned with the  $\tilde{z}$  vector of the frame  $\mathcal{E}$  (see Figure 2).

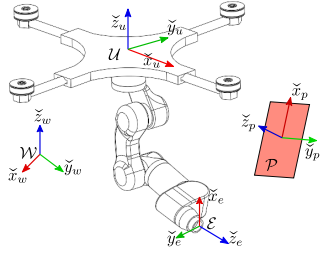


Fig. 2. Coordinate frames of a UAM system

The position  $p_{\mathcal{U}}^{\mathcal{W}} \in \mathbb{R}^3$  of the center of the aerial vehicle is measured in  $\mathcal{W}$ , while the attitude of the vehicle frame  $\mathcal{U}$  in  $\mathcal{W}$  is dictated by the roll  $\phi$ , pitch  $\theta$  and yaw  $\psi$  angles, or by the rotation matrix  $R_{\mathcal{U}}^{\mathcal{W}} \triangleq R_z(\psi)R_y(\theta)R_x(\phi)$ . The configuration of the robotic arm is represented by the vector of joint angles  $q_m \in \mathbb{R}^n$ , for a  $n$ -joint robot. All vectors in this paper are column vectors. Assuming known fixed transformation  $(p_{\mathcal{P}}^{\mathcal{W}}, R_{\mathcal{P}}^{\mathcal{W}})$  between  $\mathcal{W}$  and  $\mathcal{P}$ , the complete pose of the end-effector can be computed relative to the wall frame  $\mathcal{P}$ .

The goal is for the end-effector position and orientation to appropriately align with  $\mathcal{P}$  and subsequently exert forces along the  $\tilde{z}$  axis of  $\mathcal{P}$ . This force should be exerted at the center of  $\mathcal{P}$ . Let the position of the end-effector along the  $\tilde{z}$

axis of the wall frame be  $Z$  and  $F_d < 0$  be the desired force. The following reaction force model, as a function of the insertion into the wall,  $Z$ , is assumed<sup>1</sup>: a function  $F : \mathbb{R} \rightarrow \mathbb{R}$  that is continuous, non-decreasing and such that there exist a unique  $Z_d < 0$  such that  $F(Z_d) = F_d$ . A typical example satisfying the above assumptions is the spring-action force model:

$$F(Z) = \begin{cases} \kappa Z & \text{if } Z \leq 0 \\ 0 & \text{if } Z > 0 \end{cases}.$$

in which  $Z_d = F_d/\kappa$ . The joint motor controllers accept joint velocity references, while the aerial vehicle flight controller handles the low-level attitude control, allowing attitude and thrust setpoints to be transmitted to the autopilot. Autopilots typically accept as input the normalized thrust  $\frac{T_f}{T_m}$ , where  $T_m$  is the maximum value of  $T_f$ . Since the thrust relies on the employed brushless motor, propeller and battery characteristics, it can be introduced in the vehicle translational dynamics as an additional unknown constant.

The aerial manipulator's dynamic model is:

$$\frac{d}{dt}v_{\mathcal{U}}^{\mathcal{W}} = \frac{1}{c_m} (R_{\mathcal{U}}^{\mathcal{W}}\tilde{e}_z T_f + F_e) - g, \quad \frac{d}{dt}q_m = u_m, \quad (1)$$

where  $v_{\mathcal{U}}^{\mathcal{W}} \triangleq \frac{d}{dt}(p_{\mathcal{U}}^{\mathcal{W}})$ , and  $F_e$  is the external force vector attributed to forces exchanged with the environment and disturbances from the robotic arm. It is assumed to be upper bounded in norm by a value  $\Delta$  and also to be slow-varying  $\dot{F}_e \simeq 0$  (as in [21]). Furthermore,  $g \triangleq 9.81\tilde{e}_z$  is the gravity acceleration vector,  $q_m$  the manipulator joint position vector and  $u_m$  is the robotic arm joint velocity vector, while  $\tilde{e}_x, \tilde{e}_y, \tilde{e}_z$  are the columns of the  $3 \times 3$  identity matrix respectively.

In (1), the unknown constant  $c_m = \frac{m}{T_m}$  is related to the overall system mass  $m$ , while the rotation matrix  $R_{\mathcal{U}}^{\mathcal{W}}$  can be expressed in its corresponding Euler angles. Let the control input vector be

$$\tau = [T_f \quad \phi_d \quad \theta_d \quad \omega_z \quad u_m^{\top}]^{\top}, \quad (2)$$

where  $\omega_z$  is the angular velocity about the vehicle's  $\tilde{z}$ -axis. The controller should be designed so as to arrive at final control values  $\tau$ , while exerting a force at a selected wall-location. The controller framework is split into: a) the *high level controller* that generates the (i) UAM's linear velocity, (ii) yaw rate and (iii) the manipulator joint velocity. The latter two are sent directly as low-level commands, but the linear velocity is sent to: b) a *low level controller* that generates the appropriate remaining low level control signals.

## III. HIGH LEVEL CONTROLLER

### A. Basic definitions

In order to ensure safety during task execution, it is desired for the aerial manipulator to achieve proper alignment prior to attempting force interaction, thus avoiding undesirable collisions of parts of the system.

<sup>1</sup>  $Z < 0$  implies an insertion of the tool into the wall, whereas  $Z > 0$  means that no contact between the wall and the tool was established.

For this reason, a controller is sought, capable of guaranteeing end-effector alignment and force convergence. This controller is then combined with an appropriate control barrier function (CBF) under an optimization scheme, in order to ensure that a desirable relation between end-effector distance from the wall and end-effector alignment is maintained at all times. The devised controller outputs linear velocity and yaw angular rate commands for the aerial vehicle and joint angle velocity commands for the robotic arm, which are then transmitted to the lower-level controllers.

For the sake of simplicity, the variables in this section are expressed in the wall frame. Thus, let  $x, y, z$  the vehicle positions in  $\mathcal{P}$  (center of  $\mathcal{U}$  measured in  $\mathcal{P}$ ). As far as the high-level controller is concerned, the following *configuration vector* is defined

$$q \triangleq [x \ y \ z \ \psi \ q_m^\top]^\top. \quad (3)$$

The output command of the controller will be  $\dot{q}$  and the high-level controller assumes the dynamics  $\dot{q} = u$ , i.e.. It is also assumed implicitly that the UAM's roll( $\phi$ ) and pitch( $\theta$ ) rates are zero, as far as the high-level controller is concerned.

Let  $X(q), Y(q), Z(q)$  be the coordinates of the position of the end-effector frame and  $\tilde{x}(q), \tilde{y}(q), \tilde{z}(q)$  the orthonormal vectors of the orientation of the end-effector frame. These elements form the end-effector frame, measured in wall frame, and can be obtained using forward kinematics. Using forward differential kinematics, the linear and angular velocity geometric Jacobians  $J_v(q), J_\omega(q)$  are also defined for the end-effector frame measured in the wall frame.

According to Section II, the goal is to control the UAM to have  $X(q) = Y(q) = 0, \tilde{z}(q) = -\tilde{e}_z$  and to exert a force  $F(Z(q)) = F_d$ . The task can be separated into: a) alignment and b) force exertion, which are to be implemented using scalar potential functions.

### B. The alignment potential function

Let the positive-definite alignment function be

$$A(q) \triangleq \frac{k_x}{h} |X(q)|^h + \frac{k_y}{h} |Y(q)|^h + \frac{k_o}{g} |1 + \tilde{e}_z^\top \tilde{z}(q)|^g,$$

for constants  $h > 1, g > 1, k_x, k_y, k_o > 0$ . Note that  $A(q) = 0$  if and only if  $X(q) = Y(q) = 0$  and  $\tilde{z}(q) = -\tilde{e}_z$ . Define the symbol  $[x]^s = \text{sign}(x)|x|^s$ . The gradient of  $A$  in  $q$  will be necessary. It is given by

$$\nabla A(q) = k_x [X(q)]^{h-1} J_v(q)^\top \tilde{e}_x + k_y [Y(q)]^{h-1} J_v(q)^\top \tilde{e}_y + k_o [1 + \tilde{e}_z^\top \tilde{z}(q)]^{g-1} J_\omega(q)^\top (\tilde{e}_z \times \tilde{z}(q)).$$

### C. Force exertion potential function

Consider a continuous and non-decreasing function  $\gamma : \mathbb{R} \rightarrow \mathbb{R}$  with  $\gamma(s) = 0$  if and only if  $s = 0$ . Let:

$$U(q) \triangleq \int_{Z_d}^{Z(q)} \gamma(F(\xi) - F_d) d\xi.$$

It can be shown that  $U(q) \geq 0$  and zero if and only if  $q$  is such that  $Z(q) = Z_d$ . Furthermore,  $U(q)$  is a differentiable function on  $q$ , with  $\nabla U(q) = \gamma(F(Z(q)) - F_d) J_v(q)^\top \tilde{e}_z$ .

### D. The task Lyapunov function

Let the *high-level Lyapunov function* can be defined be

$$V_H(q) \triangleq A(q) + U(q).$$

Clearly,  $V_H(q)$  is differentiable and  $V_H(q) = 0$  if and only if  $X(q) = Y(q) = 0, \tilde{z}(q) = -\tilde{e}_z$  and  $F = F_d$  (i.e.,  $Z(q) = Z_d$ ).

### E. The distance-alignment error diagram

Given the Lyapunov function, one could consider a controller  $u = -K_q \nabla V_H(q)$  for a positive scalar  $K_q$ . However, this can be unsafe, because this controller does not consider that the UAM's manipulator can collide with the wall. To solve this issue, a *distance-alignment error* relationship will be enforced. Essentially, the distance between the end-effector and the wall  $D(q)$  and the alignment error function  $A(q)$  should follow a relationship in which there is a minimal distance  $D$  for each alignment error  $A$ , and thus the approach will happen in a safe way. Geometrically, this can be visualized by plotting  $A$  and  $D$  in a diagram, as shown in Fig. 3 and enforcing the points along the trajectory to be above a certain curve that contains the point  $A = 0, D = 0$ .

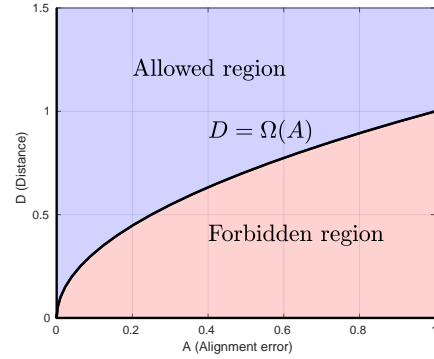


Fig. 3. Alignment error ( $A$ ) and distance ( $D$ )-diagram versus the shaping function  $\Omega(s) = \sqrt{s}$ .

For this paper, the end-effector wall-distance function is considered to be simply the distance from the end-effector point to the wall,  $D(q) \triangleq Z(q)$ . More complex distance functions, taking into the consideration the geometry of the robot, can be used if necessary. Regardless, consider a function  $\Omega$  that is differentiable, increasing and such that  $\Omega(0) = 0$ . This function will shape the distance-alignment relationship. To enforce this relationship, the *barrier distance-alignment relation function*  $B(q) \triangleq D(q) - \Omega(A(q))$  is defined, so the desired relationship can be written as  $B(q) \geq 0$ . Since that  $B$  is differentiable in  $q$ , this inequality is suitable to be enforced through CBFs with a differential inequality of the form  $\nabla B(q)^\top \dot{q} \geq -K_B B(q)$  for a positive  $K_B$ .

### F. Joint and configuration velocities limits

Limits for  $\dot{q}$  and also joint limits for the manipulator will also be enforced. Consider joint limits for the manipulator  $\underline{q}_m \leq q_m \leq \bar{q}_m$  and configuration velocity limits  $\underline{u} \leq \dot{q} \leq \bar{u}$ . The joint limits can be enforced through CBFs, and the

corresponding differential inequalities can be merged into the configuration velocity limits. Split  $\underline{u}$  and  $\bar{u}$  in its first four entries  $\underline{u}_D$ ,  $\bar{u}_D$  and remaining entries  $\underline{u}_m$ ,  $\bar{u}_m$ . Define

$$\begin{aligned} \underline{b}(q) &\triangleq [\underline{u}_D^\top \max(\underline{u}_m, K_L(q_m - \bar{q}_m))^\top]^\top \\ \bar{b}(q) &\triangleq [\bar{u}_D^\top \min(\bar{u}_m, K_L(q_m - \bar{q}_m))^\top]^\top \end{aligned} \quad (4)$$

in which  $K_L$  is a positive scalar and the maximum and minimum are taken component-wise. Then  $\underline{b}(q) \leq \dot{q} \leq \bar{b}(q)$  implements the desired constraint.

### G. The optimization problem

The QP-controller can be computed for the high-level input  $u_H$ . Define the steering controller  $u_d(q) \triangleq -K_q \nabla V_H(q)$ . The control input  $u_H$  is:

$$\begin{aligned} u_H(q) &\triangleq \arg \min_{\mu} \|\mu - u_d(q)\|^2 \text{ such that} \\ &\nabla B(q)^\top \mu \geq -K_B B(q) \\ &\underline{b}(q) \leq \mu \leq \bar{b}(q). \end{aligned} \quad (5)$$

Note that  $u_H$  is indeed a function only of  $q$ , since the reaction force is modelled to be configuration-dependent through the function  $F(Z(q))$ . However, it should be noted that *it is not necessary* to know the force-reaction model function  $F$  to compute this controller. Indeed, the force model only appears through the quantity  $F(Z(q))$ , that is part of the steering controller. This quantity can be obtained without any information about the force model provided that there is a force sensor that measures it. The mention to the force model is only necessary for the sake of the mathematical analysis.

The following results can then be shown about this controller:

*Proposition 1:* The set

$$\mathbb{P} \triangleq \left\{ q \mid B(q) > 0, \underline{q}_m < q_m < \bar{q}_m \right\} \quad (6)$$

is positive invariant.

*Proof:* The CBF constraint in (4) guarantees strict bounds  $\underline{q}_m, \bar{q}_m$  for  $q_m$ , while the first constraint of (5) guarantees  $\dot{B}(q)$  is non-decreasing as  $B(q) \rightarrow 0$ , thus ensuring positive invariance of  $\mathbb{P}$ . ■

*Proposition 2:* If the initial configuration  $q_0 \in \mathbb{P}$ , then the optimization problem is always feasible. In particular,  $\mu = 0$  is always a strictly feasible solution.

*Proof:* Application of  $\mu = 0$  in (5), results in

$$-K_B B(q) < 0, \quad \underline{b}(q) < 0 < \bar{b}(q)$$

Both of the above inequalities are already guaranteed from the positive invariance of  $\mathbb{P}$ , thus  $\mu = 0$  is a strictly feasible solution, because the  $\geq$  conditions are met with  $>$ . ■

*Proposition 3:* The solution to the optimization problem is unique.

*Proof:* From convex function theory, a strictly convex function minimized over a convex set, has a unique optimal solution (if any). In (5), the constraint set is comprised of linear inequalities and is thus convex. The quadratic

optimization problem objective function of (5) can be written in the form

$$\min_{\mu} \frac{1}{2} \mu^\top H \mu + f^\top \mu,$$

with  $H = 2I$ , where  $I$  the identity matrix and  $f = -2u_d(q)$ . Since  $H$  is positive definite, the objective function is strictly convex. ■

*Proposition 4:* For  $q \in \mathbb{P}$ ,  $u_H(q)$  is a continuous function of  $q$ .

*Proof:* The constraint functions are continuous in  $q$ . Objective function matrices  $H, f$  are also continuous in  $q$ . From [22], it can be shown that the above conditions, along with  $\mu = 0$  being a strictly feasible solution (from Proposition 2), are sufficient to prove continuity of the optimal solution  $u_H(q)$  in  $q$ . ■

*Proposition 5:* If the initial configuration  $q_0 \in \mathbb{P}$ , then for all  $t \geq 0$  the closed loop system using (5),  $\dot{q} = u_H(q)$ , is Lyapunov stable to the set  $\mathbb{V}_H \triangleq \{q \mid V_H(q) = 0\}$ , i.e.,  $\dot{V}_H = \nabla V_H(q(t))^\top u_H(q(t)) \leq 0$  for all  $t \geq 0$ .

*Proof:* Let  $G(\mu, q)$  be the objective function of (5), then by definition, the solution  $\mu = u_H(q)$  is the unique minimizer of  $G$ , or  $G(u_H(q), q) \leq G(\mu, q)$  for any feasible solution  $\mu$ .

Given  $\mu = 0$  is a feasible solution, from Proposition 2,  $G(u_H(q), q) \leq G(0, q)$  or

$$2K_q \nabla V_H(q)^\top u_H(q) \leq -\|u_H(q)\|^2 \leq 0,$$

which from the definition of  $\dot{V}_H(q)$  results in

$$\dot{V}_H(q) \leq 0. \quad \blacksquare$$

## IV. LOW LEVEL CONTROLLER

The high level controller provides the low-level variables  $\omega_z$  and  $u_m$  directly from  $u_H(q)$ . More precisely,  $\omega_z$  comes from the  $\psi$  component of  $u_H(q)$  ( $4_{th}$  element), and  $u_m$  from the  $q_m$  component of  $u_H(q)$  (last  $n$  elements). The linear velocity component of  $u_H(q)$  (the first three components), however, needs to be converted into low-level variables, which is the role of the *low level controller*. The aerial vehicle controller module needs to guarantee convergence to the desired linear velocities commanded by the CBF force controller, despite effects due to forces exchanged with the environment, as well as uncertainty in assigning vehicle thrust, as explained in Section II.

Clearly, the UAV velocity commands in  $u_H$  generated by the high-level controller in the wall frame can be directly transformed to desired velocities in the world frame, henceforth denoted by  $v_{u,d}^W$ . A control law to track this linear velocity will be shown, and its Lyapunov stability will be proved. For this purpose, some definitions are necessary. Define the velocity error,  $e_v \triangleq v_{u,d}^W - v_{u,d}^W$ . Let the variables  $\hat{F}_e, \hat{c}_m$  evolve according to the following dynamics

$$\dot{\hat{F}}_e = \sigma_p e_v - \sigma_r \sigma_p \hat{F}_e, \quad (7)$$

$$\dot{\hat{c}}_m = \sigma_m e_v^\top (K_v e_v - g) \quad (8)$$

with arbitrary initial conditions, in which  $\gamma, \sigma_p > 0$  and  $\sigma_r \geq 0$ . Furthermore, define

$$F_f \triangleq \hat{c}_m (g - K_v e_v) - \hat{F}_e, \quad (9)$$

for a positive definite matrix  $K_v \in \mathbb{R}^{3 \times 3}$ . Finally, define  $\tilde{F}_R \triangleq R_z(\psi)^\top \frac{F_f}{\|F_f\|}$ .

*Proposition 6:* If the control inputs  $T_f$ ,  $\phi_d$  and  $\theta_d$  are:

$$T_f = \|F_f\|, \phi_d = \text{asin}(\tilde{e}_y^\top \tilde{F}_R), \theta_d = \text{atan2}(\tilde{e}_x^\top \tilde{F}_R, \tilde{e}_z^\top \tilde{F}_R) \quad (10)$$

and assuming slow external disturbances  $\dot{F}_e \simeq 0$  (as in [21]) then  $e_v$  and  $\tilde{F}_e$  remain ultimately uniformly bounded.

*Proof:* Let  $\tilde{c}_m \triangleq c_m - \hat{c}_m$ ,  $\tilde{F}_e \triangleq F_e - \hat{F}_e$ , where  $c_m > 0$  and constant by definition. Define the low-level Lyapunov function  $V_L \triangleq \frac{1}{2} e_v^\top e_v + \frac{1}{2\sigma_m c_m} \tilde{c}_m^2 + \frac{1}{2c_m \sigma_p} \tilde{F}_e^\top \tilde{F}_e$ .

Note that with the choices in (10), the term  $R_{\mathcal{U}}^\top \tilde{e}_z T_f$  in (1) becomes  $F_f$ . Using (1) and (9) the Lyapunov function derivative becomes

$$\begin{aligned} \dot{V}_L = & -e_v^\top K_v e_v + \frac{\tilde{c}_m}{c_m} \left( e_v^\top K_v e_v - e_v^\top g - \frac{\dot{\hat{c}}_m}{\sigma_m} \right) + \\ & \frac{1}{c_m} \left( e_v - \frac{\dot{\hat{F}}_e}{\sigma_p} \right)^\top \tilde{F}_e, \end{aligned} \quad (11)$$

where  $\dot{\hat{c}}_m = 0$ , and  $\dot{\hat{F}}_e \simeq 0$  was used. The substitution of the adaptation evolution laws (7), (8) in (11) results in

$$\dot{V}_L = -e_v^\top K_v e_v - \frac{\sigma_r}{2c_m} (\|\tilde{F}_e\|^2 + \|\hat{F}_e\|^2 - \|F_e\|^2). \quad (12)$$

If the gain  $\sigma_r = 0$  then  $\dot{V}_L < 0$  with respect to state error variables, proving convergence of  $e_v \rightarrow 0$ . However, in the presence of unmodelled excitations [23], such adaptive controllers are prone to parameter drift, which can cause the estimates to grow unbounded despite guarantees for the tracking of error variables.

The  $\sigma$ -modification rule (i.e.,  $\sigma_r > 0$ ) is introduced to alleviate this instability in adaptations [24] by essentially regulating  $\hat{F}_e$  towards 0 as the error  $e_v$  converges to 0. Looking at (12), with  $\Delta$  upper bound of the bounded force  $\|F_e\|$  as stated in Section II then

$$\dot{V}_L \leq -\lambda_{\min}(K_v) \|e_v\|^2 - \frac{\sigma_r}{2c_m} \|\tilde{F}_e\|^2 + \frac{\sigma_r}{2c_m} \Delta^2, \quad (13)$$

in which  $\lambda_{\min}(K_v)$  is the smallest eigenvalue of  $K_v$ . Thus, the error signal  $e_v$  and estimation error  $\tilde{F}_e$  are uniformly ultimately bounded in the set

$$\mathbb{O} \triangleq \left\{ e_v, \tilde{F}_e \mid \|e_v\| \leq \sqrt{\frac{\sigma_r}{2c_m \lambda_{\min}(K_v)}} \Delta, \|\tilde{F}_e\| \leq \Delta \right\}. \quad (14)$$

Regarding initial adaptation estimates, it is straightforward for  $\hat{F}(0) = 0$  since no information about external disturbances exists at initialization. The selection of  $\hat{c}_m(0)$  is more nuanced.

Since  $c_m$  represents the thrust-to-weight ratio of the aerial vehicle (albeit in  $Kg/N$ ), a large value of  $\hat{c}_m$  signifies an initial assumption that the vehicle has a small thrust-to-weight capacity and thus the controller will start with large thrust commands. In the case where the assumption is wrong,

this behavior could result in dangerously large accelerations during take-off.

Conversely, a small value of  $\hat{c}_m$  assumes a large thrust-to-weight ratio, meaning initial thrust commands will be small. If the assumption is wrong, in this case the vehicle will simply slowly increase the thrust level as  $\hat{c}_m$  builds up and take off when the estimate becomes close enough to the real ratio. Thus, the authors suggest selecting a value of  $\hat{c}_m(0) \approx 0.02$  for any size of UAV, as it corresponds to assumed hovering thrust at just 20% of capacity, which is a significantly better ratio than any commercial type of UAV.

The overall control architecture can be found in Figure 4.

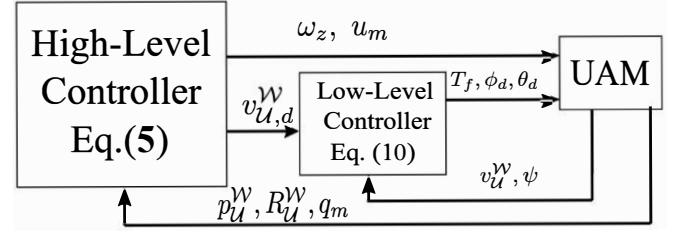


Fig. 4. Overall UAM-control block diagram.

## V. SIMULATION STUDIES

The Gazebo physics engine was employed for simulating the system along with the proposed controllers under ROS Noetic. The DJI Matrice 100 quadcopter was simulated, with the ArduCopter autopilot running in a Software-In-The-Loop configuration tasked with handling the low-level attitude control of the vehicle. A 2-DoF robotic arm is attached underneath the aerial vehicle. A screenshot from the simulator can be seen in Figure 1.

The total mass of the system is  $c_m = 2.5$  Kg. The two links of the arm have lengths  $l_1 = 0.27$  m and  $l_2 = 0.87$  m respectively, while the first joint is at 0.13 m below the center of the vehicle. The CBF gains are selected as  $k_{x,y} = 2, k_o = 1, h = g = 1.5, K_q = 0.3$ , and

Robot joint limits are  $\pm 105^\circ$  for each joint, with  $K_L = 0.35$ . Configuration velocity limits:  $\bar{u} = -\underline{u} = [0.45, 0.45, 0.35, 0.35, 0.35, 0.35]^\top$ . The force control function used is  $\gamma(F) = 0.5[F - F_d]^{0.5}$ , where  $F$  the force measured at the sensor and the alignment-barrier function  $\Omega(s) = \frac{4}{\pi} \text{atan}(1.5\sqrt{s})$ . The UAV controller gains used were  $K_v = \text{diag}(0.4, 0.4, 0.6), \sigma_m = 0.005, \sigma_p = 0.01, \sigma_r = 10^{-3}$ , with initial adaptation estimates  $\hat{F}_e = 0_{3 \times 1}, \hat{c}_m = 0.02$ . The employed units comply with SI (meters for lengths, Newtons for forces, seconds for time and rad for angles).

### A. Force Exertion Scenario

For the first simulation, the performance of the devised controller is validated while exerting force on a planar surface of arbitrary placement. Specifically, the orientation of axis  $\tilde{z}$  of  $\mathcal{P}$  is  $[-0.664, -0.664, -0.342]^\top$  when expressed in  $\mathcal{W}$ . The goal is to exert  $F_d = -3$  N of normal force. As can be seen in Figure 5 (left), the controller manages to achieve the desired force exertion. Figure 5 (right) depicts the evolution of end-effector distance from the surface ( $D(q)$ )

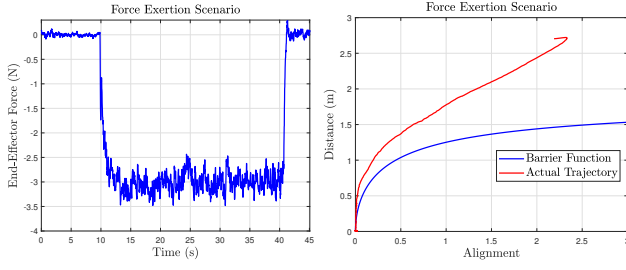


Fig. 5. Force measurement and CBF barrier constraint.

over the barrier-alignment function ( $\Omega(A(q))$ ). Clearly the CBF constraint manages to enforce the desired relationship between the two values (plotted in blue), ensuring safe force exertion.

In Figure 6 the velocity commands for the aerial vehicle generated by the optimization-based controller are plotted alongside their measured counterparts, to visualize the performance of the low-level controller of the UAV.

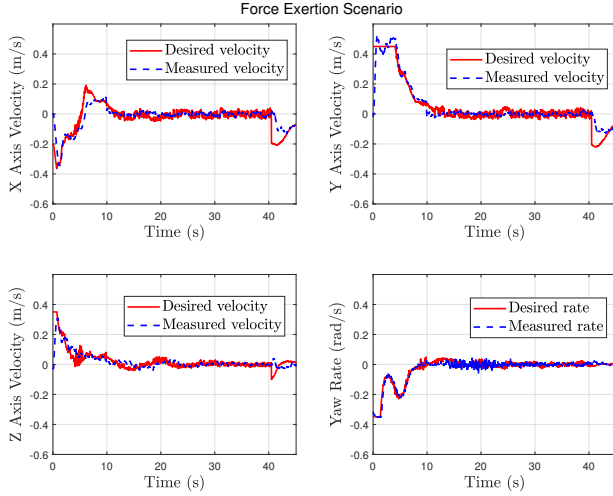


Fig. 6. Commanded and measured vehicle velocities during force exertion.

### B. Evaluation of Performance under Disturbances

In the next scenario, an external disturbance affects the yaw of the vehicle while exerting force, causing it to slip along the wall and lose contact and alignment with the environment. This is an important test in order to evaluate the capability of the designed CBF controller in overcoming such disturbances and maintaining safety during task execution.

1) *CBF Disabled:* For the first simulation, the CBF constraint in the optimization function is disabled. Without this safety-oriented action, the force controller attempts to simultaneously exert forces and correct the end-effector alignment whilst in contact with the wall, resulting in undesirable interaction with the environment and eventual loss of stability.

The force measured at the end-effector is plotted in the top of Figure 7, clearly showing failure in maintaining desired force exertion, while the bottom shows the evolution of  $D(q), \Omega(A(q))$ , with a rather large alignment error.

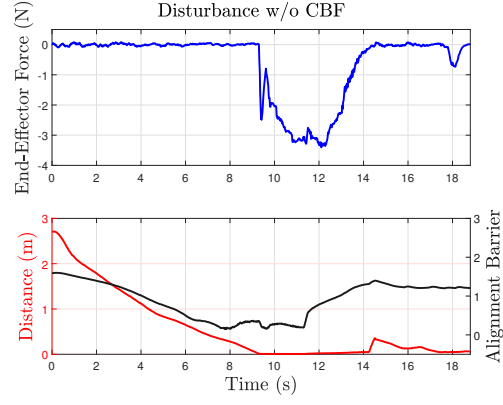


Fig. 7. Force, distance and alignment without the CBF constraint.

2) *CBF Enabled:* In contrast, Figure 8 shows that the proposed CBF controller manages to maintain a distance to the wall while recovering the end-effector's alignment, allowing for the force exertion to quickly resume safely. Figure 9 shows the evolution of distance over alignment for

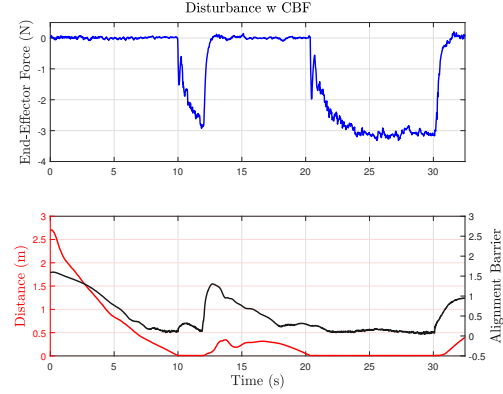


Fig. 8. Forces, distance and alignment with the CBF constraint. the same scenario. The disturbance clearly causes the barrier function to be violated and it can be seen how the controller drives the system back to the desired curve.

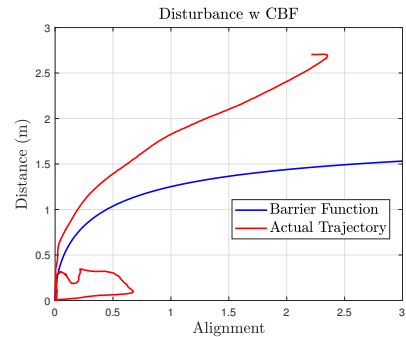


Fig. 9. Evolution of distance over alignment barrier

## VI. CONCLUSIONS

This paper presents a control architecture for force exertion on planar surfaces, with a platform consisting of an underactuated multirotor aerial vehicle and an attached robotic



arm. An optimization-based control scheme is designed, combining force measurements and a Lyapunov controller with control barrier functions, ensuring the system is capable of achieving force exertion in a prescribed, safety-oriented manner. An adaptive controller is devised for the velocity control of the aerial vehicle, guaranteeing bounded-error command tracking. The performance of the controller is validated via simulation studies.

## REFERENCES

- [1] T. Bartelds, A. Capra, S. Hamaza, S. Stramigioli, and M. Fumagalli, "Compliant aerial manipulators: Toward a new generation of aerial robotic workers," *IEEE Robotics and Automation Letters*, vol. 1, no. 1, pp. 477–483, 2016.
- [2] A. Jimenez-Cano, J. Braga, G. Heredia, and A. Ollero, "Aerial manipulator for structure inspection by contact from the underside," in *2015 IEEE/RSJ international conference on intelligent robots and systems (IROS)*. IEEE, 2015, pp. 1879–1884.
- [3] N. Michael, J. Fink, and V. Kumar, "Cooperative manipulation and transportation with aerial robots," *Autonomous Robots*, vol. 30, pp. 73–86, 2011.
- [4] D. Chaikalis, F. Khorrami, and A. Tzes, "Adaptive control approaches for an unmanned aerial manipulation system," in *2020 International Conference on Unmanned Aircraft Systems (ICUAS)*. IEEE, 2020, pp. 498–503.
- [5] N. Evangelidou, D. Chaikalis, A. Tsoukalas, and A. Tzes, "Visual collaboration leader-follower uav-formation for indoor exploration," *Frontiers in Robotics and AI*, vol. 8, p. 777535, 2022.
- [6] S. Jung, T. Hsia, and R. Bonitz, "Force tracking impedance control of robot manipulators under unknown environment," *IEEE Transactions on Control Systems Technology*, vol. 12, no. 3, pp. 474–483, 2004.
- [7] K. Gkountas, D. Chaikalis, and A. Tzes, "Force control design for a robot manipulator attached to a UAV," *IFAC-PapersOnLine*, vol. 51, no. 30, pp. 548–553, 2018.
- [8] F. Forte, R. Naldi, A. Macchelli, and L. Marconi, "Impedance control of an aerial manipulator," in *2012 American Control Conference (ACC)*, 2012, pp. 3839–3844.
- [9] G. Muscio, F. Pierri, M. A. Trujillo, E. Cataldi, G. Antonelli, F. Caccavale, A. Viguria, S. Chiaverini, and A. Ollero, "Coordinated control of aerial robotic manipulators: Theory and experiments," *IEEE Transactions on Control Systems Technology*, vol. 26, no. 4, pp. 1406–1413, 2017.
- [10] D. Chaikalis, N. Evangelidou, A. Tzes, and F. Khorrami, "Decentralized leader-follower visual cooperative package transportation using unmanned aerial manipulators," in *2023 European Control Conference (ECC)*, 2023, pp. 1–5.
- [11] S. Sharma, M. Suomalainen, and V. Kyrki, "Compliant manipulation of free-floating objects," in *2018 IEEE International Conference on Robotics and Automation (ICRA)*, 2018, pp. 865–872.
- [12] D. Smrcka, T. Baca, T. Nascimento, and M. Saska, "Admittance force-based UAV-wall stabilization and press exertion for documentation and inspection of historical buildings," in *2021 International Conference on Unmanned Aircraft Systems (ICUAS)*. IEEE, 2021, pp. 552–559.
- [13] E. Papadopoulos, F. Aghili, O. Ma, and R. Lampariello, "Robotic manipulation and capture in space: A survey," *Frontiers in Robotics and AI*, p. 228, 2021.
- [14] X. Meng, Y. He, and J. Han, "Hybrid force/motion control and implementation of an aerial manipulator towards sustained contact operations," in *2019 IEEE/RSJ International Conference on Intelligent Robots and Systems (IROS)*, 2019, pp. 3678–3683.
- [15] M. Car, A. Ivanovic, M. Orsag, and S. Bogdan, "Impedance based force control for aerial robot peg-in-hole insertion tasks," in *2018 IEEE/RSJ International Conference on Intelligent Robots and Systems (IROS)*, 2018, pp. 6734–6739.
- [16] M. Xu, A. Hu, and H. Wang, "Image-based visual impedance force control for contact aerial manipulation," *IEEE Transactions on Automation Science and Engineering*, vol. 20, no. 1, pp. 518–527, 2023.
- [17] K. Bodie, M. Brunner, M. Pantic, S. Walser, P. Pfändler, U. Angst, R. Siegwart, and J. Nieto, "Active interaction force control for contact-based inspection with a fully actuated aerial vehicle," *IEEE Transactions on Robotics*, vol. 37, no. 3, pp. 709–722, 2021.
- [18] L. Peric, M. Brunner, K. Bodie, M. Tognon, and R. Siegwart, "Direct Force and Pose NMPC with Multiple Interaction Modes for Aerial Push-and-Slide Operations," in *2021 IEEE International Conference on Robotics and Automation (ICRA)*, 2021, pp. 131–137.
- [19] G. Nava, Q. Sablé, M. Tognon, D. Pucci, and A. Franchi, "Direct force feedback control and online multi-task optimization for aerial manipulators," *IEEE Robotics and Automation Letters*, vol. 5, no. 2, pp. 331–338, 2020.
- [20] A. D. Ames, S. Coogan, M. Egerstedt, G. Notomista, K. Sreenath, and P. Tabuada, "Control barrier functions: Theory and applications," in *2019 18th European Control Conference*, 2019, pp. 3420–3431.
- [21] S. Kim, H. Seo, S. Choi, and H. J. Kim, "Vision-guided aerial manipulation using a multirotor with a robotic arm," *IEEE/ASME Transactions On Mechatronics*, vol. 21, no. 4, pp. 1912–1923, 2016.
- [22] B. Morris, M. J. Powell, and A. D. Ames, "Sufficient conditions for the lipschitz continuity of qp-based multi-objective control of humanoid robots," in *52nd IEEE Conference on Decision and Control*, 2013, pp. 2920–2926.
- [23] P. A. Ioannou and P. V. Kokotovic, "Instability analysis and improvement of robustness of adaptive control," *Automatica*, vol. 20, no. 5, pp. 583–594, 1984.
- [24] E. Lavretsky and K. A. Wise, "Robust adaptive control," in *Robust and adaptive control: With aerospace applications*. Springer, 2012, pp. 317–353.